Cerebellar granule cells acquire a widespread feedback control signal during motor learning

Andrea Giovannucci[1,2 †], Aleksandra Badura[1,3 †], Ben Deverett[1,4], Farzaneh Najafi[5,*] Talmo D. Pereira[1], Zhenyu Gao[6], Ilker Ozden[1,7], Alexander D. Kloth[1,**], Eftychios Pnevmatikakis[2,8], Liam Paninski[8], Chris I. De Zeeuw[3,6]
Javier F. Medina[9], Samuel S.-H. Wang[1]

[1]Princeton Neuroscience Institute and Department of Molecular Biology, Princeton University, Princeton, NJ, USA. [2]Simons Center for Data Analysis, Simons Foundation, New York, NY, USA.[3]Netherlands Institute for Neuroscience, Amsterdam, The Netherlands. [4]Robert Wood Johnson Medical School, New Brunswick, NJ, USA. [5]Department of Biology, Univ. of Pennsylvania, Philadelphia, PA, USA. [6]Department of Neuroscience, Erasmus MC, Rotterdam, The Netherlands. [7]Department of Physics and Division of Engineering, Brown University, Providence, RI, USA. [8]Departments of Statistics and Neuroscience, Columbia University, New York, New York, USA. [9]Department of Neuroscience, Baylor College of Medicine, Houston, TX, USA.

* Current address: Cold Spring Harbor Laboratory, Cold Spring Harbor, NY, USA.
** Current address: University of North Carolina, Chapel Hill, NC, USA.
† Equal contributions.

Correspondence: Samuel S.-H. Wang
Princeton Neuroscience Institute, Washington Road
Princeton University
Princeton, NJ 08544
Tel: (609) 258-0388
Email: sswang@princeton.edu

Javier F. Medina
Department of Neuroscience
Baylor College of Medicine
One Baylor Plaza, Room S709
Houston, TX 77005
Tel: (713) 798-8141
Email: jfmedina@bcm.edu

Abstract: Cerebellar granule cells, which constitute half the brain's neurons, supply Purkinje cells with contextual information necessary to guide corrective actions. However, little is known about how granule cells encode this information. Here we show, using two-photon microscopy for tracking neural activity in head-fixed mice, that granule cell populations develop a dense representation of the corrective response. Over multiple days of conditioning, we monitored granule cell populations in a region whose activity plays a role in modulating learned eyeblinks. During the first few days, granule cells responded to neutral visual and somatosensory stimuli, as well as the unconditional periorbital airpuff used for training. As learning progressed, approximately two-thirds of the monitored granule cells acquired a conditional response whose timing matched or slightly preceded the protective eyelid movement. Individual granule cell activity co-varied trial by trial to form a redundant code. Many of the same granule cells were also active during spontaneous movements of nearby body structures. Thus a movement-related feedback signal is readily and widely available at the input stage of the cerebellar cortex, as required by forward models of cerebellar control over action.

The cerebellum is widely recognized as supporting associative learning necessary for generating predictive and corrective actions in specific contexts[1]. Contextual information is thought to be encoded at the input level of the cerebellum in the granule cell (GrC) population[2], and may include peripheral and internally generated sensory signals[1,3,4], as well as feedforward signals about a learned motor command[5,6]. However, little is known about actual GrC representations during the learning process because cerebellar learning is

slow[7] and single-cell recording methods only allow GrCs to be monitored on a single day for a brief period of time[8-10].

The question of how GrCs represent contextual information during behavior can be understood in terms of several models of cerebellar information processing. In one longstanding hypothesis, contextual information is provided by a very small fraction of granule cells (GrCs), speculatively as few as ~1%[3]. During associative learning, such subpopulations of GrCs have been suggested to represent externally-generated conditional stimuli (CSs) such as tones or light flashes[11].The pairing of CSs with an unconditional stimulus (US) such as a corneal airpuff triggers learning processes in which the resulting changes in CS-driven Purkinje cell spiking drive a well-timed blink that protects the eye – a conditional response (CR)[11].

Alternatively, in the domain of continuous actions such as smooth movements, the cerebellum has also been suggested to convey a broader range of information as part of a feedback system for control of overall brain output[12,13]. In forward models for motor control, it is suggested that the outcomes of actions are continually being predicted, with the prediction being fed back within the brain, as part of a dynamic process of adjustment[12]. Such models require that GrC inputs to the cerebellum convey not only external-world information such as CSs, but also internally generated predictions of action, on an ongoing basis.

We tested these ideas about neural representations in GrCs by using two-photon microscopy of GCaMP6f to image populations of GrCs while mice underwent classical eyeblink conditioning in a head-fixed apparatus. This combination of methods allowed us to follow the evolution of learned GrC representations over many days.

Results

We expressed the calcium indicator protein GCaMP6f in cerebellar lobule VI (**Figure 1a**) using two adeno-associated virus type 1 (AAV1)-based strategies. In wild-type mice we injected an AAV1 construct that used the human synapsin promoter to drive widespread expression in the granule cell layer[14]. In Neurod1-Cre mice from the laboratory of M.E. Hatten, we used a conditional strategy by injecting AAV1-Flex-GCaMP6f. Both strategies led to widespread expression in the granule cell layer (**Figure 1b** and **Extended Data ED1**). Regions-of-interest (ROIs) to be monitored were selected by criteria of near-circularity and 4.5-7.5 μm diameter, often with an annular pattern of fluorescence. Positive staining for the granule-cell-specific $GABA_A$ alpha6 subunit was found in 99.7±0.1% of such ROIs in both hSyn-injected and Neurod1-Cre mice, indicating that virtually all monitored structures belonged to GrCs. 94±2% of all ROIs were DAPI-positive at the center, completing their identification as GrC somata. No mossy fiber-like structures were observed to express GCaMP. Larger, DAPI-positive/alpha6-negative structures were occasionally observed and tentatively classified as Golgi or Lugaro cells (**Extended Data ED1).** Thus, our *in vivo* imaging criteria predominantly identify individual GrC somata (**Figure 1c**).

In two Neurod1-Cre mice we further confirmed GrC expression by imaging at molecular-layer locations. We observed axon-like structures and boutons (**Figures 1d** and **1e**). These structures were active in the absence of any applied stimuli and responded to corneal airpuffs and light flashes (**Figure 1f and Supplementary Movie ED2**). Signals from rows of mediolaterally aligned boutons were strongly correlated (**Figure 1d**), consistent with a common origin from a shared parallel fiber and indicative of the propagation of action potentials.

In brain slices, we measured GrC somatic fluorescence signals while evoking and monitoring action potentials electrically via mossy fiber stimulation or patch electrode (**Extended Data ED3).** We recorded action potentials in cell-attached mode to prevent GCaMP washout, which occurs during whole-cell recording. Fluorescence signal amplitude increased monotonically as a function of the number of mossy fiber stimuli (**Extended Data ED3b**) as well as action potentials, up to the highest number of spikes tested, 20 spikes at 50-600 Hz (**Extended Data ED3c**). In published observations of *in vivo* activity recorded during awake behavior, including locomotion[9] and whisker stimulation[10], brief high-frequency bursts have been observed (10-14 spikes at 40-170 Hz[9] and 1-25 at 270-440 Hz[10], respectively). In this range of activity in brain slices, we found that the fluorescence increase ranged from $\Delta F/F_0$=24% to 155% (**Extended Data ED3c**, gray area shows spiking activity recorded by Powell *et al.*). In our experiments *in vivo* calcium imaging of 268 granule cells whose activity was highly correlated with locomotion (r >0.6; N=5 mice) revealed $\Delta F/F_0$ signals ranging from 23 to 165%. Thus GCaMP signals *in vivo* are consistent with expectations from published electrophysiological observations of GrC activity.

For *in vivo* imaging (**Supplementary Movie ED4**) of learned representations, we followed 128 GrCs for up to 12 days of training in 3 mice (**Extended Data ED5),** and 268±91 granule cells in fields of view re-imaged over one or more sessions without one-to-one cell match in 3 more mice (97 fields of view). To investigate granule cell representations we used classical eyeblink conditioning (**Figure 2a**), a form of Pavlovian learning that requires cerebellar activity and plasticity[15,16]. Mice were trained by pairing a conditional stimulus (CS) in the form of a flash of light (N=4) or a weak airpuff to the

ipsilateral whisker area (N=2) with an aversive unconditional stimulus (US), a peri-orbital airpuff which reliably evoked an unconditional reflex blink (UR; **Figure 2b**). After repeated pairings of the CS and US over the course of multiple conditioning sessions, the CS-alone came to elicit an anticipatory conditional eyeblink response (CR) that started before the time of the expected US onset and is part of a broader avoidance response[17]. By the end of training, CRs were elicited on an average of 73±13% (range 58-96%) of all the trials and CR amplitude reached 43±7% of the US-triggered full eyelid closure (**Figure 2c**).

In all mice (N=6), we imaged GrCs near the surface of cerebellar lobule VI (**Figure 1a**), an optically accessible region that, although not previously included among known regions necessary for conditioning[7,18,19], mediates movements of nearby trunk and neck regions (**Extended Data ED6**) and is likely to be engaged during eyeblink conditioning, because it receives climbing fiber inputs triggered by the periorbital airpuff US[20,21]. Indeed, in separate non-imaging experiments with five mice that were trained to a high level of conditional responses (%CR > 70%), we found that injection of muscimol in the same region of cerebellar cortex led to a reversible reduction in CR probability and amplitude (**Figure 2d and e**). CRs decreased from 81%±5% of UR amplitude (mean±standard deviation) during the baseline measurements, to 39%±19% of UR amplitude (**Figure 2d**), an effect that was not seen after control injections of saline in the same animals (72%±6%; different from muscimol injection, p=0.005; CR amplitude smaller in muscimol condition than saline injection, p=0.026). The degree of reduction increased with the size of the injected area within anterior-lateral lobule VI (**Extended Data ED7**) indicating that this region plays a significant role in modulating the production of learned blinks.

Figure 3 shows trial-by-trial recordings of calcium signals in a single GrC along with simultaneously recorded behavioral responses over the course of 9 days of conditioning using a CS (light CS, **Figure 3a**; whisker CS, **Extended Data ED8**). To demix and denoise somatic signals from the surrounding neuropil we used structured matrix factorization methods[22] (**Supplementary Movie ED4**). In addition to measuring eyelid closure (**Figure 3b**, left), we used computer-assisted analysis of video recordings to calculate treadmill speed (**Figure 3a** and **Figure 3b** middle) and whisker/snout movement (**Figure 5**). These algorithms allowed us to resolve movements with single-frame resolution (**Extended Data ED9, Supplementary Movies ED10 and ED11**).

To assess the relationship between behavioral and cellular responses, we divided all data into trials in which only the periorbital puff was delivered (US), trials in which the animal produced no CR and showed no significant locomotion (speed < 2 cm/s) during the CS presentation (CR^-; **Figure 3b**, top row), and trials in which the mouse produced a CR but showed no significant locomotion (speed < 2 cm/s) during the CS presentation (CR^+; **Figure 3b**, middle row). The example neuron highlights three features of GrC responses. First, the US evoked a large calcium response in all trials (**Figure 3b**, bottom, cyan trace and **Extended Data ED8b**). This response was consistent with drive either from activation of somatosensory inputs from the peri-orbital area, or from motor signals linked to the reflex blink or high levels of movement. Second, presentation of the CS evoked a smaller calcium response that was detectable even on trials with no CR and no significant locomotion (**Figure 3b**), suggesting that it could have been driven either by sensory inputs or by undetected movements. Third, individual GrC responses were substantially larger on CR^+ trials than on CR^- trials (**Figure 3b** and **Extended Data ED8b**), an effect that could be explained by activation of CR-related inputs. Thus, this example granule cell was active

during eyeblink conditioning and carried a signal correlated with the presence or absence of the CR.

If GrC calcium signals are related to CRs, they would be expected to have temporal dynamics that match the eyelid response, and to grow in amplitude with learning (**Figure 4**). For both light and whisker CS (**Figure 4a**), the eyelid response and average GrC population activity showed correlated changes in peak time (**Extended Data ED12a-b**). In GrCs with a correlation with CR amplitude of greater than 0.3, the signal preceded the start of eyelid closure by 68±28 ms (185 neurons, 4 mice; **Extended Data ED12b**), consistent with a predictive control signal and ruling out sensory reafference as the sole mechanism.

To test whether GrC responses grew with learning we examined calcium responses and behavioral output across training days (**Figure 4b**). We quantified the magnitude of eyelid movement (*e**, **Figure 4a**) and GrC calcium response (*f**) in CR^+ and CR^- trials in an 85-msec time window preceding the UR. Figure 4b shows how calcium signals evolved over the course of 9 days of conditioning for one field of view comprising 29 GrCs. In individual GrCs (**Figure 4b**, top), CR^+-associated calcium responses grew with training while CR^-associated responses did not. Calcium signals in CR+ trials increased in parallel with eyelid closure amplitude (**Figure 4b**, bottom, purple points), while overall average animal locomotion was below 0.05 cm/s (**Figure 4b**, bottom, green points). We obtained similar results in all the other fields of view (N=6 mice), after accommodating for the learning dynamics of the different animals by binning GrC activity according to the level of performance (Figure 4c). Thus, across the population of GrCs, the average f* increased progressively for low, medium, and high probability CR epochs (**Figure 4c and Extended Data ED12c**; left panel Pearson's $r=0.21\pm0.04$, $p<0.001$ and right panel $r = 0.12\pm0.04$,

p<0.01; mean±SD from bootstrapping procedure), indicating that learning is accompanied by the emergence of a CR-specific GrC signal.

Analysis of calcium responses in populations of granule cells revealed that most GrCs were activated by the CS in CR- trials (**Figure 4d** and **Extended Data ED12d**, 1 field of view per mouse, red bars), and also carried a CR-related signal (defined as the difference of the f* signal between CR+ and CR– trials, black bars in **Figure 4d** and **Extended Data ED12d**). In fact, when we inspected individual granule cells across all fields of view in all mice (N=6) we found that most of them (64±18%) carried this CR-related signal (the trial-by-trial activity was significantly correlated with the eyelid response, see methods for details).

Our custom matrix factorization algorithm[22] recognized 58±18 GrCs per 10000 μm^2. Based on a total density of 187±27 GrCs per 10000 μm^2 as determined by histological analysis, this corresponds to an estimated 31±10% of all GrCs. Thus, at a minimum, 0.64*31%=21% of all GrCs within the field of view encoded contextual information during the CS period, substantially more than the 1% predicted by mainstream theoretical models.

Because optogenetic activation of the imaged area of lobule VI resulted in neck, trunk, and limb movements (**Extended Data ED6)**, we surmised that GrC activity in this region might be associated with actions other than the production of learned blinks. Indeed, we found GrCs with calcium signals that were correlated with eyelid movement, wheel speed, or snout movement (**Figure 5a**). We quantified these correlations computing the Pearson's r coefficient between the GrC signals and behavior (**Figure 5b** for an example cell correlated with eyelid movement during CR, and **Figure 5c** for an example cell correlated with eyelid movement during UR). In addition, some individual GrCs showed activity that correlated with multiple movement parameters (**Figure 5d**). To categorize each

GrC according to its preferred movement parameter, we identified the one movement (eyelid-CR, snout, wheel, or eyelid-UR) that was most highly correlated with its calcium signal. In animals that reached the advanced stage of training and with behavioral data available (>60% conditional responses, N=3 mice), more GrCs were best correlated with eyelid-CR than with any of the other movements (**Figure 5e**).

The strong correlation between calcium signals and behavior in many individual GrCs suggests that the code may be redundant at the level of the population. To test for redundancy in GrC representations, we used the previously computed Pearson's correlation values for eyelid-CR to calculate the degree to which individual and multiple GrCs could encode a single, well-quantified movement parameter, CR amplitude. A linear regressor based on the activity of all the GrCs in the population was more correlated with CR amplitude than any single GrC (**Figure 6a**, compare gray shaded zone with red distribution), indicating that the CR is more accurately encoded by a distributed representation of GrC activity.

We quantified the degree of redundancy across the GrC population by computing the regressor's capacity to predict CR amplitude trial-by-trial. Capacity was measured in units of Shannon mutual information between the regressor output and the eyelid trace. Mutual information increased with the number of neurons included in the regressor (**Figure 6b**), but rapidly reached a plateau as more neurons were added. The amount of redundancy in the GrC population was calculated using a redundancy index $\mathbf{\Lambda}$, which was defined as the upper bound of information contained in the neurons individually, divided by the amount of information contained in the population regressor. When all imaged neurons were included, the median value of $\mathbf{\Lambda}$ was 12 (range, 7 to 140, N=6 mice), exceeding levels seen elsewhere in the central nervous system[23,24]. $\mathbf{\Lambda}$ increased proportionally with the

number of GrCs monitored (r=+0.89) and since many active GrCs were not imaged in our experiments, the true degree of redundancy is likely to be even higher.

Discussion

Our findings demonstrate that neural activity related to learned movements is available at the input stage of cerebellar cortex, and in a notably high fraction of granule cells. This signal may arise from cells in the anterior interpositus nucleus that increase their firing during the CR[25]. Deep nuclear activity can lead to net excitation of granule cells by two routes: monosynaptic excitation, via collaterals of principal cells which terminate as mossy fibers[26,27]; and disynaptic disinhibition, via inhibitory deep nuclear neuron projections onto Golgi cells, which in turn inhibit granule cells[28]. Descending information may also arrive in cerebellum via corticopontine pathways, which can converge onto the same granule cells as sensory pathways[29]. It has been suggested that the cerebellum may use signals like those we have uncovered as a form of efference copy to compute forward models that overcome the problems associated with long delays in sensory feedback[12,13]. In this way the duality between driving behavioral output and receiving a copy of the output may allow the cerebellum to participate in a closed feedback loop that regulates and adjusts ongoing predictive responses in real time[13].

Single GrCs could be activated during multiple distinct movements with specificity that was often, but not always, restricted to eyelid, snout, or locomotion. These correlations describe a representation of both unconditional and conditional movement and are consistent with the idea that the mossy fiber pathway in this region of lobule VI provides a stream of information that is available for the generation and control of movements by separate but nearby body structures[30].

Traditional theories of cerebellar function[3] emphasize that the pattern of connectivity and the staggering number of granule cells in the cerebellar cortex makes these cells perfectly suited to produce high-dimensional representations, in which each context is encoded by a unique pattern of activity in the granule cell population, and a slight change in context strongly alters the pattern of activity. Marr's theory suggests that (a) individual cells should fire only rarely and (b) the activity of granule cells should be uncorrelated[30]. Until now, these predictions have never been tested directly because of a lack of ability to monitor activity in a population of granule cells, especially during a cerebellum-dependent task. Our evidence does not match these classical predictions. Instead, we observed contextual, redundant activity, consistent with a dense representation[30].

We found that by the end of training, granule cell population responses were strongly dependent on whether a CR was produced. The population response contained temporal components that both precede and come simultaneously with the motor command. This brings up the possibility that granule cell populations act as a source of behavioral variation. Previously, it has been found that the firing rate of individual Purkinje cells is highly correlated with learned movements on a trial-by-trial basis[32,33], suggesting that the firing of entire Purkinje cell populations must be highly correlated. Our finding of population-level covariation in granule cell firing suggests that in the production of cerebellar-driven movements, Purkinje cell populations could derive their correlation from the fact that they receive input signals that are themselves highly correlated[34].

Since inhibition of the imaged locations leads to disruptions in learned blink amplitude, the observed learning-related neural responses in GrCs may drive Purkinje cell responses in lobule VI and its neighboring regions in simplex lobule and anterior vermis contribute to eyeblink conditioning, autonomic responses that accompany conditioning[17],

and neck, trunk, and forelimb defensive movements[7,31]. In such a cerebellar region capable of forming multiple, related associations, redundancy might help the system amplify its learned blink response[27] as well as increase its ability to discriminate between[35,36], and generalize to, new stimuli[4]. In this way a copy of the learned output may help the cerebellum to refine an action as brief as an eyeblink, even as it is produced.

Acknowledgements. This work was supported by National Institutes of Health grants R01 NS045193 (S.W.) and R01 MH093727 (J.M.), New Jersey Council on Brain Injury Research fellowship CBIR12FEL031 (A.G.), the Searle Scholars program (J.M.), DARPA N66001-15-C-4032 (L.P.), National Science Foundation Graduate Research Fellowship DGE-1148900 (T.P.), the Nancy Lurie Marks Family Foundation (S.W.), by the Dutch Fundamental Organization for Medical Sciences (ZonMW; C.I.D.Z.), Life Sciences (NWO-ALW; C.I.D.Z.), and Social and Behavioral Sciences (NWO-MAGW; C.I.D.Z.), as well as ERC-adv and ERC-POC (C.I.D.Z.). A.G. designed behavioral+imaging experiments, established the behavioral and imaging set-up and molecular methods, performed *in vivo* imaging experiments, developed analyses, and drafted the manuscript. A.B., Z.G. and C.I.D.Z. designed and/or performed brain slice, histological, and combined behavioral-pharmacological experiments. F.N., I.O., B.D., and A.K. established the behavioral and imaging setup and methods. B.D. performed *in vivo* imaging experiments and developed analyses. T.P., E.P., and L.P. developed analyses. J.M. and S.W. designed experiments and developed analyses. All authors edited the manuscript. The authors thank Laura Lynch for expert laboratory assistance, A.C.H.G. Ijpelaar for technical assistance and Dr. H. Boele of the Neuroscience department at the Erasmus Medical Center for their input in eyeblink recordings, Michael J. Berry II for discussion of the information calculation, Daniel Dombeck, John Peter Rickgauer and Cristina Domnisoru for experimental advice, and Diego Pacheco-Pinedo, Jessica L. Verpeut, Paloma Sanchez-Jauregui and Ilana Witten for comments and suggestions.

METHODS

Animal preparation for in vivo two-photon calcium imaging

Experimental procedures were approved by the Princeton University Institutional Animal Care and Use Committee and performed in accordance with the animal welfare guidelines of the National Institutes of Health. Details of animal preparation were modified from previously published procedures[20]. For imaging experiments we used 5 male, 12- to 16-week-old C57BL/6J mice (Jackson Laboratory) and 2 male, 20-week-old B6.Cg-Tg.NeuroD1-Cre.GN135Gsat mice. All mice were group-housed in reversed light cycle. During the surgery mice were anesthetized with isoflurane (5% for induction, 1.0-2.5% for maintenance) and a 3-mm-wide craniotomy was opened. A custom-made two-piece headplate[20], with a removable part to allow repeated access for viral injections, was attached to the animal's head. To increase stability, the skull was thoroughly cleaned in the region surrounding the target imaging zone (lobule VI of the cerebellar vermis) and except for the craniotomy zone, the skull surface was covered with Metabond (Parkell, S380) prior to opening a craniotomy. For imaging experiments, after an overnight delay for animal recovery, the top plate was removed for delivery of 400-800 nL (~50 nL/minute) of virus (for C57BL/6J mice, AAV1.Syn.GCaMP6f.WPRE.SV40 virus [Penn Vector Core, lot AV-1-PV2822]; for NeuroD1 mice, AAV1.CAG.Flex.GCaMP6f.WPRE.SV40) in two injections ~750 and ~1250 μm lateral to the midline and 250 μm deep from the dura surface using borosilicate glass pipettes (World Precision Instruments, 1B100F-4, 1/0.58 mm OD/ID) beveled to 30 degrees with a 10-20 μm tip opening. In 2 mice craniotomies and injections were performed during the same surgery and an imaging window was implanted and glued onto the skull, and a standard aluminum headplate was cemented to

the skull for the purpose of head fixation. All animals were placed back in their home cage for 2 weeks of recovery.

Habituation and eyeblink training for chronic experiments

Two to three weeks after AAV injections, animals were trained as previously described[7]. Animals were first habituated to a freely-rotating treadmill for repeated intervals over at least 5 days of graded exposure. After habituation was complete, animals were trained while simultaneously measuring brain activity under a two-photon microscope. To minimize the learning time, animals were trained for up to 4 short sessions per day. The number and duration of training sessions were varied according to the type of conditional stimulus (CS) and the behavioral state of the animal. If an animal showed signs of discomfort, it was returned to its home cage for up to 24 hours. The unconditional stimulus (US) was a periorbital airpuff (10-20 psi, 30 ms in duration, delivered via a plastic needle placed 5 mm from the cornea and pointed at it). The conditional stimulus was a flash of light (400 nm, "light CS", 500 ms, contralateral to the US) or an airpuff to whisker vibrissae (2-3 psi, "whisker CS", 800 ms, ipsilateral to the US). In experiments using light CS, the CS-US interval was 250 ms from CS start to US start, and training spanned 7-12 days. In experiments using whisker-puff CS the CS-US interval was 440 ms since vibrissa stimulation allowed for larger inter-stimulus intervals; learning was faster[7] and training spanned 6 days.

Identification of imaging zone

At the beginning of the first day of measurements, a CS-responsive cerebellar zone was identified by delivering 10 CS-US paired stimuli while imaging zones in the vermis of

lobule VI, between the midline and the paravermal vein. The average fluorescence response to the CS in the zone was computed during the experiment using a custom ImageJ (http://imagej.nih.gov) macro, and zones showing >20% ΔF/F were selected for further imaging. CS-US pairings were used in order to prevent delays in learning that can arise from latent inhibition caused by non-reinforced pre-exposure to the CS[37]. For later recording sessions, the field of view was matched first by using surface landmarks such as blood vessels, then by using the brain surface overlying the imaging zone for further localization, and finally by comparing the fluorescent field of view itself with previous sessions.

Data acquisition

Behavioral data was collected using custom software in Python [www.python.org]. In the first set of experiments, imaging data was collected using ScanImage version 3.8.1 (Vidrio Technologies). Behavioral acquisition software on one computer sent triggering signals to drive a National Instruments USB card (PCIe 6363) on a second computer for image acquisition. Calcium imaging was acquired at 128x64 pixels per frame at 15.6 Hz or 128x128 at 3.9 Hz (64 or 256 ms per frame, 1 ms per line, bidirectional scanning) and behavioral data at 320x240 pixel movies at 100 Hz (Sony PS3 Eye, interfaced with custom software written in Python). Imaging and behavioral data were collected in 4-second epochs per trial. Within each trial, the CS stimulus was delivered 1.92 seconds (baseline activity) after the starting trigger. To synchronize data, ScanImage channel 2 was used to record the eyelid signal output from the Python module and channel 3 was used to record CS, CS-US, and US triggers.

In the second set of experiments, imaging data was collected using ScanImage 2015 (Vidrio Technologies). Behavioral acquisition software on one computer sent triggering and synchronization signals via a National Instruments card (USB 8451) to a second computer for image acquisition. Calcium imaging was acquired at 512x512 pixels per frame at 29 Hz, and behavioral data at 320x240 pixel movies at 60 Hz (Sony PS3 Eye, interfaced with custom software written in Python). Data were collected in 8-second epochs. Within each trial, the CS stimulus was delivered 4 seconds after the starting trigger. To synchronize data, an I2C-based synchronization protocol was used to send trial timing information from the behavior acquisition computer to the imaging computer in real time.

The number of trials per session depended on the animal stress level, and ranged from 25 to 100 trials. Eyelid position was extracted from the movies collected with the PS3 camera. During training, eyelid closure was measured as the integral of a manually defined zone enclosing the eye. Animal self-motion and locomotion were estimated from camera images through a custom-built image processing pipeline (see **Behavioral tracking**). Each trial was initiated only if the animal was still, the eyelid was open, and an interval of at least 12 seconds had elapsed from the previous trial. Thresholds for eyelid closure and movement were set from baseline signals at the time of the experiment.

Channelrhodopsin-2 stimulation

B6.Cg-Tg(Thy1-COP4/EYFP)18Gfng/J mice (Jackson Laboratories, 007612) expressing ChR2 under the Thy-1 promoter were implanted with an optical window as described above. After one week of recovery, they were habituated to the treadmill. Using an Olympus 4x macro objective (NA=0.28 and WD=29.5 mm) light from a blue LED (470 nm, LUXEON Rebel, #SP-03-B4) was focused ~200-400 μm under the cerebellum surface

(125-250 mW/mm^2). 10-50 stimuli of 10 ms duration and 50 Hz frequency were delivered at different locations (crus I and II, lobules V, VI, and simplex) of cerebellar surface. Movements were extracted as the frame-on-frame value among motion components, calculated as the squared inter-frame pixel difference averaged across manually selected regions of interest (limbs, whiskers, oral, trunk-neck) from high-speed infrared movies.

Offline analysis of blinks

CR^+ (CR^-) trials were identified as responses greater (smaller) than 10% of the full blink in a window from 50 msec before to 30 msec after the US trigger. Trials with only US presentation or CS presentation were termed US and CS-alone trials.

Behavioral tracking

To isolate the effect of unrelated self-motion and/or proprioceptive sensory activity we developed an image processing pipeline to extract quantitative measures of motor behaviors from videos recorded through a high framerate camera positioned in front of (but not orthogonal to) the animal. As a proxy for locomotion, wheel velocity was estimated through a model-based approach to tracking wheel motion. First, a model of the wheel was constructed by measuring the physical dimensions of the uniformly spaced bumps (nubs) on the wheel surface. A simplified representation of the wheel (Figure ED10, Movie ED11) was then manually registered to the surface of a minimally occluded region of the wheel. This enabled the calculation of a projective transformation matrix that corrects for the perspective distortion introduced by the non-orthogonal positioning of the behavior camera. The reprojected videos were contrast-normalized via CLAHE[38] and an ROI was selected such that there was again minimal occlusion from the animal's body. Then, HOG features[39]

centered at each pixel in the ROI were extracted as a way to describe the appearance of the local image region. This proved robust to differences in illumination artifacts and particularly to heterogeneity in the wheel's texture. Extracted features were matched across subsequent frames by finding the nearest neighbor with a ratio of its Euclidean distance to that of the next nearest neighbor of at least 0.7. This matching procedure reduces the rate of ambiguous matches by ensuring they are sufficiently distinct, but does not guarantee that there will be matches between frames; for these, linear interpolation was used to fill in missing data. Finally, the wheel velocity was estimated from the median displacement in the ROI converted to physical units by scaling to the wheel model.

To measure self-motion in the form of movement of snout and whisker muscles in the absence of locomotion or wheel displacement, we devised a method for tracking a set of manually selected seed points along the contour of the animal's snout with the assumption that most self-motion would result in changes in its shape (Figure ED10, Movie ED12). The snout was automatically segmented from the background using Otsu's method[40] to find an optimal threshold to separate distributions in the image intensity histograms. The points along the boundary of the mask were then used as candidate points for matching to the original seed points that trace the contour of the snout. As these motions were highly nonlinear and segmentation did not always result in perfect separation from the background, matching was achieved via Coherent Point Drift[41], a robust point set registration algorithm. Matching was performed across frames by selecting the closest contour-line point subject to rigidity constraints in deformation of the seed contour. The contour line traces were then used as trajectories of the snout shape used to estimate displacements in pixels/sec. As imaging conditions varied greatly across videos, a secondary pipeline was developed to process videos that could not be tracked using the

aforementioned method. For these cases an ROI was selected such that only the upper part of the snout of the animal and no wheel pixels were included. This region was tiled into evenly spaced blocks (12x12 pixels) and matched across frames via normalized cross-correlation, i.e., "block matching". Tracking the trajectories of each block enabled comparable results as the shape-based approach, but may not include subtle motions of the tip of the snout.

Calcium imaging data analysis

Image data analysis was performed using custom MATLAB, Python and ImageJ scripts. Movies were processed in batches containing a maximum of 18000 frames and were fragmented in case changes in FOVs were too dramatic. As a first step, movies were motion-corrected using the *template matching and slice alignment* ImageJ plugin [https://sites.google.com/site/qingzongtseng/template-matching-ij-plugin], which is based on the *opencv* matching template function, or an equivalent Python implementation for the second set of experiments. For slow scan (i.e. < 25 Hz), in order to compensate for warping induced by brain movement and scanning microscopy, we separately corrected for motion the top and bottom portion of each movie and then stitched them back together. For the first batch of experiments, prior to matrix factorization, movies were preprocessed to set a baseline of 0 and a range of 0-1. Slow changes in the pixel fluorescence time series were removed by examining the distribution of fluorescence in a ±5 s interval around each sample time point and subtracting the 8th percentile value[14]. Finally, the movies were normalized to a range of 0 to 1. For the second batch, we used an updated version of CNMF that did not suffer from arbitrary signal scale or baseline.

For regions of interest identification, we used an algorithm for calcium image source separation based on nonnegative matrix factorization (NMF[22]). The algorithm is specialized for separating signals from overlapping structures by relying on the fact that signals from different structures often have different time signatures. This algorithm allowed removal of activity from diffuse sources, a pattern consistent with ascending axons passing through neuropil (Extended Data, Movie ED4). The resulting estimate of neuropil activity was removed from the movie, and of the regions of interest, a subset was selected that corresponded to granule cells. The neuropil-subtracted movie was renormalized to F values and traces were extracted using the selected regions of interest. $\Delta F/F_0$ was computed as previously[14] except using baseline (F_0) extracted using NMF. In slow scanning experiments, temporal precision was corrected using the relationship between scanning position and time, to remap each field of view to true time within the frame. When possible, neurons were matched across days or sessions (N=4 mice). To match neurons across days, we wrote a special purpose script to align fields of view from different days using the *template matching and slice alignment* ImageJ plugin and then match the regions by maximizing an intersection over union metric (cells were matched when the ratio of overlapping pixels vs. total pixels was maximal). Imaging and behavioral data were synchronized by resampling both signals to 30 Hz, and aligning them based on the eyelid and trigger signals. Cells of the same identity were confirmed by exact location across days in 3 animals, and aggregated population analysis was done in 3 animals whose field of view changed slightly over multiple days (N=2) or were imaged only after training (N=1). The criteria for selecting granule cells were based on the size (4.5 um – 7.5 um), the location within the brain (under the Purkinje cell layer), and the range of activity (max range 400%

DF/F). In the first batch granule cells were selected manually (N=4 mice) and in the second automatically (N=2 mice).

$\Delta F/F_0$ traces were aligned to the delivery of stimuli (0 seconds being the time of expected US), and the median value during baseline (1 second preceding CS or US stimulus delivery) was subtracted from the waveform.

Correlation computation

In order to quantify the similarity between granule cell activities and behavioral responses, We firstly aligned and binned in 100 msec bins behavior and fluorescence. Then, correlation between neural activity and snout or wheel dynamics was quantified with the Pearson's r coefficient between neural activity and granule cell activity excluding the window of stimulus delivery (between 500 msec before and 1500 msec after the US). In order to compute the regressor between neural activity and CR or UR responses, the same correlation above was applied during the stimulus delivery time: -500 msec to 35 msec after US for CR correlation and from 35 before to 750 msec after the US for UR. In order to estimate the confidence interval for correlation we repeated the procedure above but shuffling the trials and than taking the 95th percentile of the distribution as threshold.

Multivariate linear regression

In order to probe the redundancy in the population code, we implemented a multivariate linear regressor that was trained using half of the trials randomly selected, and then evaluated on the remaining half. The regressor was implemented by the scikit **sklearn.linear_model.LinearRegression [http://scikit-learn.org/stable/modules/generated/sklearn.linear_model.LinearRegression.html]**. This corresponds to the

regression of an n-dimensional response on a matrix of predictor variables, with normally distributed, potentially heteroscedastic and/or correlated, errors. The regressor was run 100 times on different random subdivisions of trials (50% training and test sets), giving rise to a distribution of solutions. The fitness of each solution was quantified by computing the correlation coefficient between the predicted and actual values of the eyelid magnitude (e*) in test trials (**Figure 4c**, black and gray). To test the redundancies of the neural code, we trained it on smaller subsets of neurons to assess the performance degradation (**Figure 4d** top, black), and compared its performance to the highest-correlation cell in the remaining subpopulation (**Figure 4d** top, black vs. red).

Redundancy calculation

Redundancy was quantified by dividing the maximum possible amount of Shannon information present in GrC population activity by the actual amount of information that is found in GrC-based predictions of CR amplitude. The mutual information between the regressor (or a single-neuron signal) prediction and eyeblink output amplitudes was calculated as $I_{CL} = -1/2\ log_2\ (1-r^2)$, where r is the Pearson correlation coefficient between the predicted and actual eyeblink amplitude, calculated on a trial-by-trial basis. This expression is equivalent to $I_{CL} = 1/2\ log_2(v/v_\delta)$, where v is the variance in eyelid position across trials and v_δ is the residual variance that is unexplained by the regressor or single-neuron signal. The redundancy was calculated as $\mathbf{\Lambda} = \sum I_i / I_{regressor}$, where the summation occurs across all individual neurons.

Statistics

Most of the statistics and grouping were performed using Python pandas[http://pandas.pydata.org/]. Values in text are reported as mean ± standard deviation unless otherwise indicated. When reported, p-values are calculated employing two-tailed unpaired or paired t-tests. Regarding the assumption of normality, pooled across all trials, blink amplitudes and granule-cell fluorescence signals appeared bimodal. Responses were therefore sorted into responding (CR+) and nonresponding (CR-) trials. All the statistics on neural activity or behavior were calculated only if at least ten cells or at least 8 trials were available per FOV or session, excepting the case of UR related computation, where the number was lowered to 4 trials. Because we imaged anywhere from 30 to 400 GrCs per mouse, bootstrapping with 30 granule cells per animal was done to obtain a uniformly distributed sample across mice (**Extended Data ED12c**).

Histological procedures

Mice were anesthetized with pentobarbital and perfused with 4% paraformaldehyde. Brains were isolated and processed as previously described[42,43]. In short, following perfusion brains, were incubated in 10% sucrose, embedded in gelatin, rapidly frozen, sectioned coronally at 40 µm and collected in 0.1M PB. Sections were processed for immunohistology by washing with PBS and incubation in a blocking buffer (10% normal horse serum, 0.5% Triton in PBS) prior to a three-day incubation at 4 °C in PBS buffer containing 2% NHS, 0.4% Triton and the following primary antibodies: brains from mice used in the cerebellar-inactivation/muscimol study (n=5) were stained for Zebrin-/Zebrin+ bands using goat anti-Aldolase C antibody (sc-12065; Santa Cruz Biotechnology, 1:1000);

brains from mice used for granule cell identification and counts (n=4; two C57BL/6J injected with AAV1.Syn.GCaMP6f.WPRE.SV40 virus and two B6.Cg-Tg.NeuroD1-Cre.GN135Gsat mice injected with AAV1.CAG.Flex.GCaMP6f. WPRE.SV40. Viral injections and surgeries were performed as described above. One of the NeuroD1 mice used for histological studies was first used for in vivo calcium imaging experiments (Figure 1e)) were stained with rabbit anti-α6GABAA receptor antibody (G0295; Sigma, 1:1000). Next, sections were washed in PBS, incubated for 2 hours at room temperature in PBS buffer with secondary antibodies, counter stained with DAPI for 10 minutes (30 µl/ml) and mounted on glass slides with Vectashield anti-fade mounting medium (H-1000; Vector laboratories, USA). Alexa Fluor488-conjugated donkey anti-goat secondary antibody was used to visualize Adolase C immunoreactivity (Jackson ImmunoResearch, West Grove, PA; Invitrogen; 1:200), and Alexa Fluor633-conjugated goat anti-rabbit secondary antibody (Jackson ImmunoResearch, West Grove, PA; Invitrogen; 1:200) was used on brains incubated with rabbit anti-α6GABAA receptor primary antibody. Sections stained for immunofluorescence were scanned with a Leica SP8 confocal laser-scanning microscope (Leica Microsystems, Germany) using 10x, 40x and 63x objectives, hybrid (HyD) detectors for sensitive detection, and sequential scan mode.

Characterization and quantification of GCaMP-positive cells

Cerebella of hSyn and Neurod1 animals were sectioned coronally at 40 µm and processed for immunofluorescence staining of the α6GABAA receptor and counterstained with DAPI as described above. All quantifications were performed manually in randomly selected fields of view (FOV) of 10^4 μm^2 using the ImageJ plugin Cell Counter. For each section, DAPI-positive cells were counted and scored for the expression of GCaMP and co-staining

of α6GABAA receptor. Next, GCaMP-positive structures with cell-like characteristics (round shape, >4.5 μm), but without DAPI counterstain were scored and analyzed for co-staining of α6GABAA receptor. For quantification cells were subdivided into two groups according to size, 4.5-7.5 μm and >7.5 μm, and further characterized as follows: (a) Granule cells: α6GABAA receptor-positive, DAPI positive and 4.5-7.5 μm in size; (b) Non-granule cells: DAPI-positive, GCaMP-positive structures >7.5 μm; (c) "Potential" granule cells: GCaMP-positive, DAPI-negative structures of 4.5-7.5 μm in size. Because of the limited number of cells >7.5 μm, to get a better estimate, we included counts of complete lobules (tile scan; ~25x bigger FOV) and normalized the counts to a FOV of 10^4 μm^2.

Acute brain slice experiments

Mossy fiber stimulation recordings and calcium imaging of granule cells: 7 Male, six-week-old C5B7L/J6 mice were anesthetized with isoflurane and injected in lobule VIb with AAV1.Syn.GCaMP6f.WPRE.SV40 virus as described in Animal preparation paragraph. Four to five weeks later, 250 μm-thick sagittal cerebellar brain slices were prepared using ceramic blades (Lafayette Instrument Co., Lafayette, IN) on a vibratome (VT1000S, Leica, Germany) set to speed 1.0–2.5 and frequency 8–9) under immersion in oxygenated ice-cold (~4°C) artificial CSF (aCSF) containing (in mM) 126 NaCl, 3 KCl, 1 NaH_2PO_4, 20 D-glucose, 25 $NaHCO_3$, 2 $CaCl_2$, and 1 $MgCl_2$. Brain slices were preincubated at 34°C for 40–60 min, then kept at room temperature. For recording, slices were transferred to an immersion-type recording chamber perfused at 2–4 ml/min with oxygenated aCSF at ~34°C. For extracellular mossy-fiber stimulation, a large patch electrode filled with aCSF was positioned at the surface of the slice in the. Granule cells were imaged using a custom-

built two-photon laser scanning microscope using pulsed 900-nm excitation from a Ti:sapphire laser (Mira 900, Coherent). Excitation power was kept below 15 mW at the backplane of the objective (40X, NA 0.8 IR-Achroplan; Carl Zeiss, Thornwood, NY). Data acquisition was controlled by ScanImage v 3.6.1 (Vidrio Technologies).

Loose patch recordings/stimulation and calcium imaging of granule cells: 8 male mice were used. Unless reported, animal and slice preparation was done as described above. Cerebella were removed and dissected in ice-cold oxygenated slicing medium containing (in mM): 93 N-methyl-D-glucamine, 93 HCl, 2.5 KCl, 5 sodium ascorbate, 2 thiourea, 3 sodium pyruvate, 0.5 $CaCl_2$, 10 $MgCl_2$, 30 $NaHCO_3$, 1.2 NaH_2PO_4, 20 HEPES, and 25 D-glucose (mOsm 300, pH 7.4). 250 μm sagittal slices of the vermis were cut on a vibratome (VT2000S, Leica, Germany). Slices were incubated in slicing medium at near physiological temperature (34°C) for 2 mins and transferred to 34°C aCSF for 30 mins. Subsequently slices were held in a chamber filled with oxygenated aCSF at room temperature covered with aluminum foil to prevent too much light exposure and used within 6 hours. Experiments were performed in aCSF at near physiological temperature ~33°C. Loose cell attached recordings were performed under a multiphoton microscope (A1R MP+, Nikon, Japan) and Axon Multiclamp 700A amplifier. The patch pipettes (7-9 MΩ) were filled with intracellular solution containing (in mM): 120 potassium gluconate, 9 KCl, 10 KOH, 3.48 $MgCl_2$, 4 NaCl, 10 HEPES, 4 Na_2ATP, 0.4 Na_3GTP, 17.5 sucrose and 10-20 μm Alexa 594 (at pH 7.25). To reliably elicit action potential firing in granule and Golgi cells, 1 ms, 100-200 mV of voltage steps were delivered through the patch pipettes. Imaging data was collected using an NIS-Elements Software (Nikon Instruments). Signals were synchronized by using imaging software as an external trigger for the Axon Multiclamp 700A amplifier. Calcium imaging was acquired at 30 Hz (1 ms per line,

bidirectional scanning).

Cerebellar inactivation experiments

5 male C5B7L/6J mice were equipped with a cranial 3-mm-wide window covered by a silicone plug (Kwik-Sil, WPI) and a custom-made two-piece headplate (see Animal preparation paragraph for details). Following a three-day recovery period, mice were habituated and trained in the custom-built eyeblink setup described before[35,44]. Mice were habituated to a freely-rotating treadmill for repeated intervals over the period of 5 days. After habituation, animals were trained for one up to 1 hour a day for a period of 11 days.

The unconditional and conditional stimulus (US and CS, respectively) were delivered as described above. For conditional stimulus flash of light (400 nm, "light CS", 500 ms, contralateral to the US) was used for all conditional mice. On average mice received 220 trials per day (200 CS-US paired trails and 20 CS only probe trials). After 11 days of training all mice reached stable performance level (CR production ~80%). On day 12 the first inactivation experiment was performed. Mice first received 110 baseline trials (100 CS-US paired trails and 10 CS only trials), next they were taken out of the setup, lightly anesthetized with Isoflurane and fixed in a stereotactic frame. The silicone plug was removed and 100 nl injections of either a 0.5% muscimol (Tocris with 1% Evans blue) dissolved in sterile saline (0.9% NaCl, Hospira) or the vehicle (saline) were made in the same coordinates, which were used for imaging neural responses. In order to reach the granule cell layer and ensure the reproducibility of the injection size, injections were made ~300µm deep from the surface of the brain using a Nanoject II Auto-Nanoliter Injector (Drummond Scientific Company, USA). After injections the brain was covered with the plug, mice were placed back in the setup, and after 15 min recovery time they were

subjected to 110 eyeblink conditioning trails (100 CS-US paired trials and 10 CS only trials). The next day (day 13) the inactivation experiment was repeated but the drug/vehicle condition was switched, meaning that mice, which received saline on day 12 were injected with 0.5% muscimol, and mice which were injected with the drug received the vehicle. Immediately after acquiring the post-injection trials an overdose of sodium-pentobarbital (0.15 mL i.p.) was administered allowing transcardial perfusion (0.9% NaCl followed by 4% paraformaldehyde in 0.1 M phosphate buffer (PB); pH=7.4) to preserve the tissue for histological verification of the injections.

Data sharing

Code and raw data are available on request.

References

1 Ito, M. Cerebellar circuitry as a neuronal machine. *Progress in Neurobiology* **78**, 272-303, doi:10.1016/j.pneurobio.2006.02.006 (2006).

2 Arenz, A., Bracey, E. F. & Margrie, T. W. Sensory representations in cerebellar granule cells. *Current Opinion in Neurobiology* **19**, 445-451, doi:10.1016/j.conb.2009.07.003 (2009).

3 Marr, D. A theory of cerebellar cortex. *Journal of Physiology* **202**, 437-470 (1969).

4 Spanne, A. & Jorntell, H. Questioning the role of sparse coding in the brain. *Trends in Neurosciences* **38**, 417-427, doi:10.1016/j.tins.2015.05.005 (2015).

5 Blakemore, S. J., Wolpert, D. M. & Frith, C. D. Central cancellation of self-produced tickle sensation. *Nature Neuroscience* **1**, 635-640, doi:10.1038/2870 (1998).

6 Houck, B. D. & Person, A. L. Cerebellar premotor output neurons collateralize to innervate the cerebellar cortex. *Journal of Comparative Neurology* (2015).

7 Heiney, S. A., Kim, J., Augustine, G. J. & Medina, J. F. Precise control of movement kinematics by optogenetic inhibition of Purkinje cell activity. *The Journal of Neuroscience* **34**, 2321-2330, doi:10.1523/JNEUROSCI.4547-13.2014 (2014).

8 Eccles, J., Faber, D., Murphy, J., Sabah, N. & Táboříková, H. Afferent volleys in limb nerves influencing impulse discharges in cerebellar cortex I. In mossy fibers and granule cells. *Experimental Brain Research* **13**, 15-35 (1971).

9 Powell, K., Mathy, A., Duguid, I. & Hausser, M. Synaptic representation of locomotion in single cerebellar granule cells. *eLife* **4**, doi:10.7554/eLife.07290 (2015).

10 van Beugen, B. J., Gao, Z., Boele, H. J., Hoebeek, F. & De Zeeuw, C. I. High frequency burst firing of granule cells ensures transmission at the parallel fiber to purkinje cell synapse at the cost of temporal coding. *Frontiers in Neural Circuits* **7**, 95, doi:10.3389/fncir.2013.00095 (2013).

11 Medina, J. F. & Mauk, M. D. Computer simulation of cerebellar information processing. *Nature Neuroscience* **3 Suppl**, 1205-1211, doi:10.1038/81486 (2000).

12 Shadmehr, R., Smith, M. A. & Krakauer, J. W. in *Annual Review of Neuroscience* Vol. 33 89-108 (2010).

13 Wolpert, D. M., Miall, R. C. & Kawato, M. Internal models in the cerebellum. *Trends in Cognitive Sciences* **2**, 338-347 (1998).

14 Ozden, I., Dombeck, D. A., Hoogland, T. M., Tank, D. W. & Wang, S. S.-H. Widespread state-dependent shifts in cerebellar activity in locomoting mice. *PLoS one* **7**, e42650, doi:10.1371/journal.pone.0042650 (2012).

15 Freeman, J. H. & Steinmetz, A. B. Neural circuitry and plasticity mechanisms underlying delay eyeblink conditioning. *Learning & Memory* **18**, 666-677, doi:10.1101/lm.2023011 (2011).

16 Boele, H. J., Koekkoek, S. K. & De Zeeuw, C. I. Cerebellar and extracerebellar involvement in mouse eyeblink conditioning: the ACDC model. *Frontiers in Cellular Neuroscience* **3**, 19, doi:10.3389/neuro.03.019.2009 (2010).

17 Thompson, R. F. & Krupa, D. J. Organization of memory traces in the mammalian brain. *Annual Review of Neuroscience* **17**, 519-549, doi:10.1146/annurev.ne.17.030194.002511 (1994).

18 Hesslow, G. Correspondence between climbing fibre input and motor output in eyeblink-related areas in cat cerebellar cortex. *Journal of Physiology* **476**, 229-244 (1994).

19 Mostofi, A., Holtzman, T., Grout, A. S., Yeo, C. H. & Edgley, S. A. *Journal of Neuroscience* **30**, 8920-8934 (2010).

20 Najafi, F., Giovannucci, A., Wang, S. S.-H. & Medina, J. F. Sensory-driven enhancement of calcium signals in individual Purkinje cell dendrites of awake mice. *Cell Reports* **6**, 792-798, doi:10.1016/j.celrep.2014.02.001 (2014).

21 Najafi, F., Giovannucci, A., Wang, S. S.-H. & Medina, J. F. Coding of stimulus strength via analog calcium signals in Purkinje cell dendrites of awake mice. *eLife* **3**, e03663, doi:10.7554/eLife.03663 (2014).

22 Pnevmatikakis, E. A. *et al.* Simultaneous denoising, deconvolution, and demixing of calcium imaging data. *Neuron* (2016).

23 Narayanan, N. S., Kimchi, E. Y. & Laubach, M. Redundancy and synergy of neuronal ensembles in motor cortex. *Journal of Neuroscience* **25**, 4207-4216, doi:10.1523/JNEUROSCI.4697-04.2005 (2005).

24 Puchalla, J. L., Schneidman, E., Harris, R. A. & Berry, M. J. Redundancy in the population code of the retina. *Neuron* **46**, 493-504, doi:10.1016/j.neuron.2005.03.026 (2005).

25 Freeman, J. H. Cerebellar learning mechanisms. *Brain Research* **1621**, 260-269, doi:10.1016/j.brainres.2014.09.062 (2015).

26 Houck, B. D. & Person, A. L. Cerebellar premotor output neurons collateralize to innervate the cerebellar cortex. *Journal of Comparative Neurology* **523**, 2254-2271, doi:10.1002/cne.23787 (2015).

27 Gao, Z. *et al.* Excitatory cerebellar nucleocortical circuit provides internal amplification during associative conditioning. *Neuron* **89**, 645-657, doi:10.1016/j.neuron.2016.01.008 (2016).

28 Ankri, L. *et al.* A novel inhibitory nucleo-cortical circuit controls cerebellar Golgi cell activity. *eLife* **4**, doi:10.7554/eLife.06262 (2015).

29 Huang, C. C. *et al.* Convergence of pontine and proprioceptive streams onto multimodal cerebellar granule cells. *eLife* **2**, e00400, doi:10.7554/eLife.00400 (2013).

30 Jorntell, H. Cerebellar physiology: links between microcircuitry properties and sensorimotor functions. *Journal of Physiology*, doi:10.1113/JP272769 (2016).

31 Lee, K. H. *et al.* Circuit mechanisms underlying motor memory formation in the cerebellum. *Neuron* **86**, 529-540, doi:10.1016/j.neuron.2015.03.010 (2015).

32 Medina, J. F. & Lisberger, S. G. Variation, signal, and noise in cerebellar sensory-motor processing for smooth-pursuit eye movements. *Journal of Neuroscience* **27**, 6832-6842, doi:10.1523/JNEUROSCI.1323-07.2007 (2007).

33 ten Brinke, M. M. *et al.* Evolving models of pavlovian conditioning: cerebellar cortical dynamics in awake behaving mice. *Cell Reports* **13**, 1977-1988, doi:10.1016/j.celrep.2015.10.057 (2015).

34 Lisberger, S. G. & Medina, J. F. How and why neural and motor variation are related. *Current Opinion in Neurobiology* **33**, 110-116 (2015).

35 Billings, G., Piasini, E., Lorincz, A., Nusser, Z. & Silver, R. A. Network structure within the cerebellar input layer enables lossless sparse encoding. *Neuron* **83**, 960-974, doi:10.1016/j.neuron.2014.07.020 (2014).

36 Vonderschen, K. & Chacron, M. J. Sparse and dense coding of natural stimuli by distinct midbrain neuron subpopulations in weakly electric fish. *Journal of Neurophysiology* **106**, 3102-3118, doi:10.1152/jn.00588.2011 (2011).

37 Lubow, R. E. Latent inhibition. *Psychological Bulletin* **79**, 398-407 (1973).

38 Zuiderveld, K. Bilinear Coons patch image warping. *Graphics Gems IV Graphics Gems* (ed P.S. Heckbert) Ch. VIII.5, 474-485 (Academic Press Professional, Inc., 1994).

39 Dalal, N. & Triggs, B. Histograms of oriented gradients for human detection. *IEEE Computer Society Conference on Computer Vision and Pattern Recognition.* 886-893.

40 Otsu, N. A threshold selection method from gray-level histograms. *IEEE Transactions on Systems, Man, and Cybernetics* **9**, 62-66 (1979).

41 Myronenko, A. & Song, X. Point set registration: Coherent point drift. Pattern Analysis and Machine Intelligence. *IEEE Transactions on Pattern Analysis and Machine Intelligence.* **32**, 2262-2275 (2010).

42 Badura, A. *et al.* Climbing fiber input shapes reciprocity of Purkinje cell firing. *Neuron* **78**, 700-713, doi:10.1016/j.neuron.2013.03.018 (2013).

43 Jaarsma, D. *et al.* A role for Bicaudal-D2 in radial cerebellar granule cell migration. *Nature Communications*, doi:doi:10.1038/ncomms4411 (2014).

44 Kloth, A. D. *et al.* Cerebellar associative sensory learning defects in five mouse autism models. *eLife* **4**, e06085, doi:10.7554/eLife.06085 (2015).

Figure 1

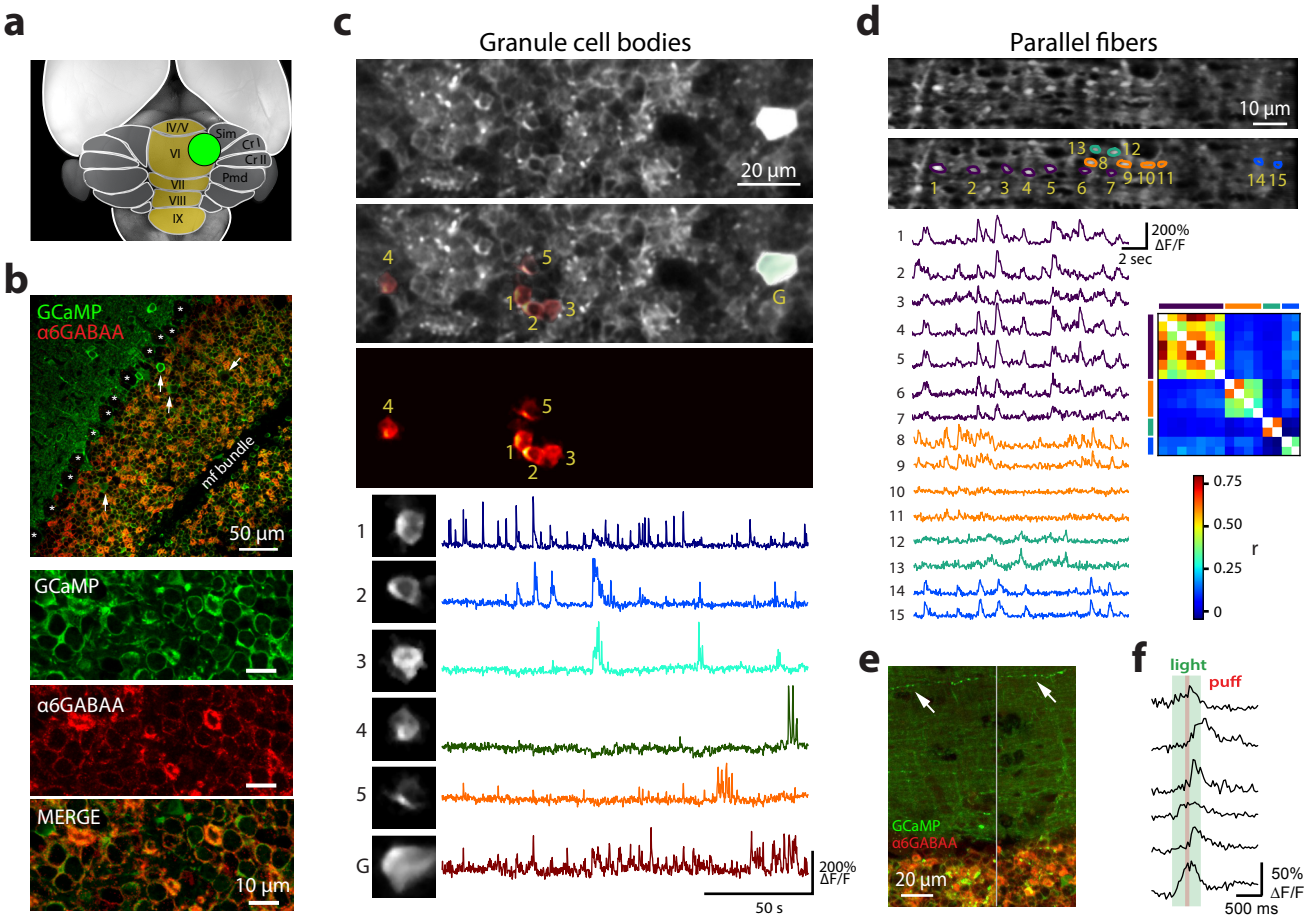

Figure 1: GCaMP expression and signals in cerebellar granule cells.
(**a**) Dorsal view of cerebellum with imaged area of lobule VI indicated in green. (**b**) α6GABAA staining (red) highlights dense expression of GCaMP6f (green) in granule cells (GrCs). Note the absence of GCaMP signal in the mossy fiber (mf) bundle. (**c**) *Top*. *Three panels show* i) two-photon imaging field of view in the granular layer, ii) overlaid with a subset of spatial components identified by NMF and classified as granule cells (shaded red) or a putative Golgi cell (green), and iii) same granule cells on a dark background. *Bottom*. GrC fluorescence traces and corresponding spatial mask. (**d**) Two-photon imaging of parallel fiber activity. *Top*. Two panels show a field of view without and with manually selected regions of interest. *Lower left*, fluorescence traces. *Lower right,* cross-correlations reveal high correlation between mediolaterally aligned boutons. (**e**) Coronal cerebellar sections of the mouse shown in panel d, counterstained for α6GABAA. Arrows point to a parallel fiber expressing GCaMP6f. (**f**) Fluorescent traces from parallel fiber boutons recorded from a trained mouse, aligned to corneal airpuffs and light flashes.

Figure 2

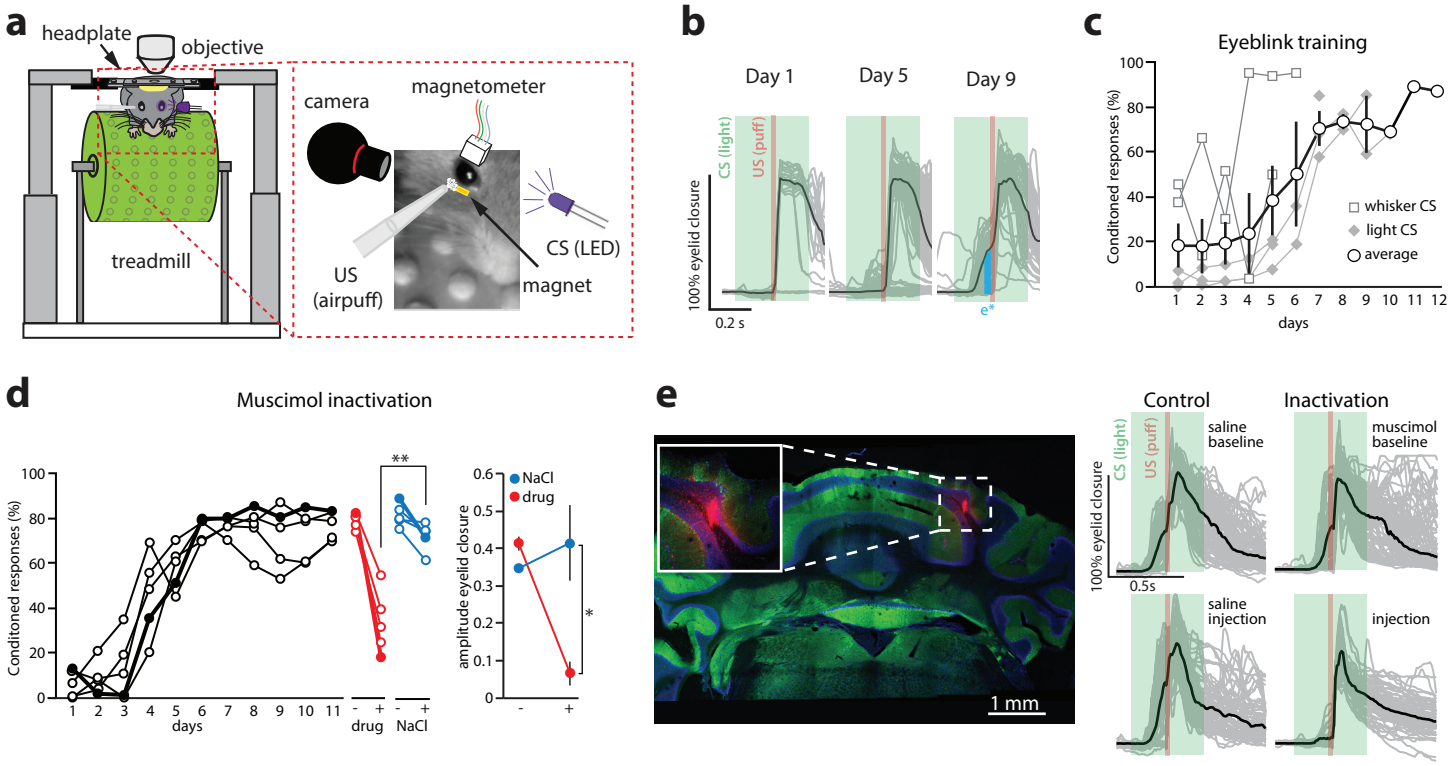

Figure 2: Role of imaged regions in eyeblink conditioning.
(**a**) Task schematic. Conditional stimuli (CS, UV LED flash to the contralateral eye or weak puff to the ipsilateral vibrissa) and unconditional stimuli (US, periorbital airpuff) were delivered to a head-fixed mouse on a freely-moving treadmill while blinks, snout and body movement, and treadmill rotation were monitored by high-speed infrared camera (100 frames/s) or a magnet attached to the lower eyelid. (**b**) Conditional responses (CRs), quantified as eyelid closure as a fraction of US response, during CS-US paired trials in a single animal. Green (CS, light) and red (US, airpuff) shaded zones indicate stimulus presentations. Blue shaded zone indicates time window for computing e*, a measure of CR amplitude. (**c**) Evolution of learning in 6 animals trained for up to 12 consecutive days. (**d**) Focal injection of muscimol but not saline vehicle led to a reduction in the percentage and amplitude of CRs. (**e**) Example of the inactivation experiment in one mouse. *Left,* a coronal cerebellar section counterstained with DAPI (blue) and aldolase C (green) reveal the injection position (red, muscimol plus Evans Blue). *Right,* individual (light gray) and averaged (black) eyelid responses during baseline trials before injections, and after drug or saline injections.

Figure 3

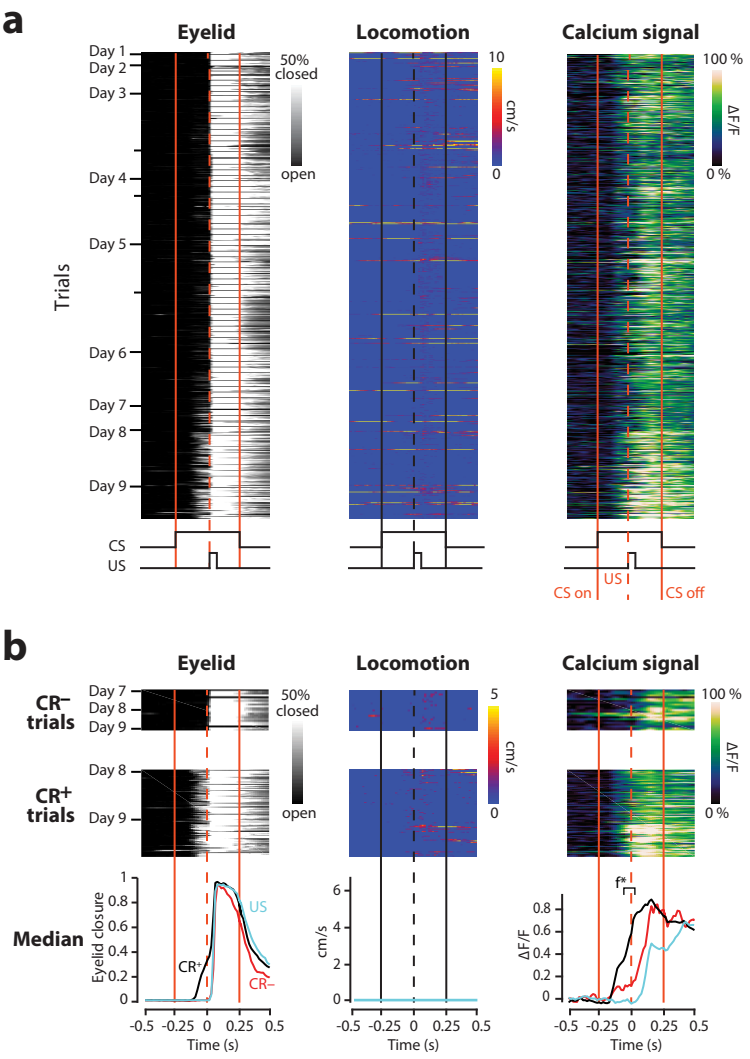

Figure 3: Calcium signals of a single granule cell during eyeblink conditioning.
(**a**) Eyelid movement (left), locomotion activity (center), and single-cell calcium signal (right) over nine days of training. Each horizontal line represents a single trial. Date labels indicate the start of a day's training, and unlabeled ticks indicate the start of a new session within the same day. Vertical solid lines indicate onset and offset of CS stimulus. Dashed vertical lines indicate delivery time of the US stimulus. (**b**) *Top.* Data from the last three days of training, re-sorted according to whether the CS did ("CR$^+$", middle) or did not ("CR$^-$", top) evoke an anticipatory eyelid closure prior to the US. Trials with significant locomotion (> 2 cm/s) during the CS are excluded. *Bottom.* Overlaid average responses in US trials (US, cyan), and at the final stage of training when the animal did ("CR$^+$", black) or did not ("CR$^-$", red) produce a CR. f* is the integral of the neural response in an 85 ms window before the UR.

Figure 4

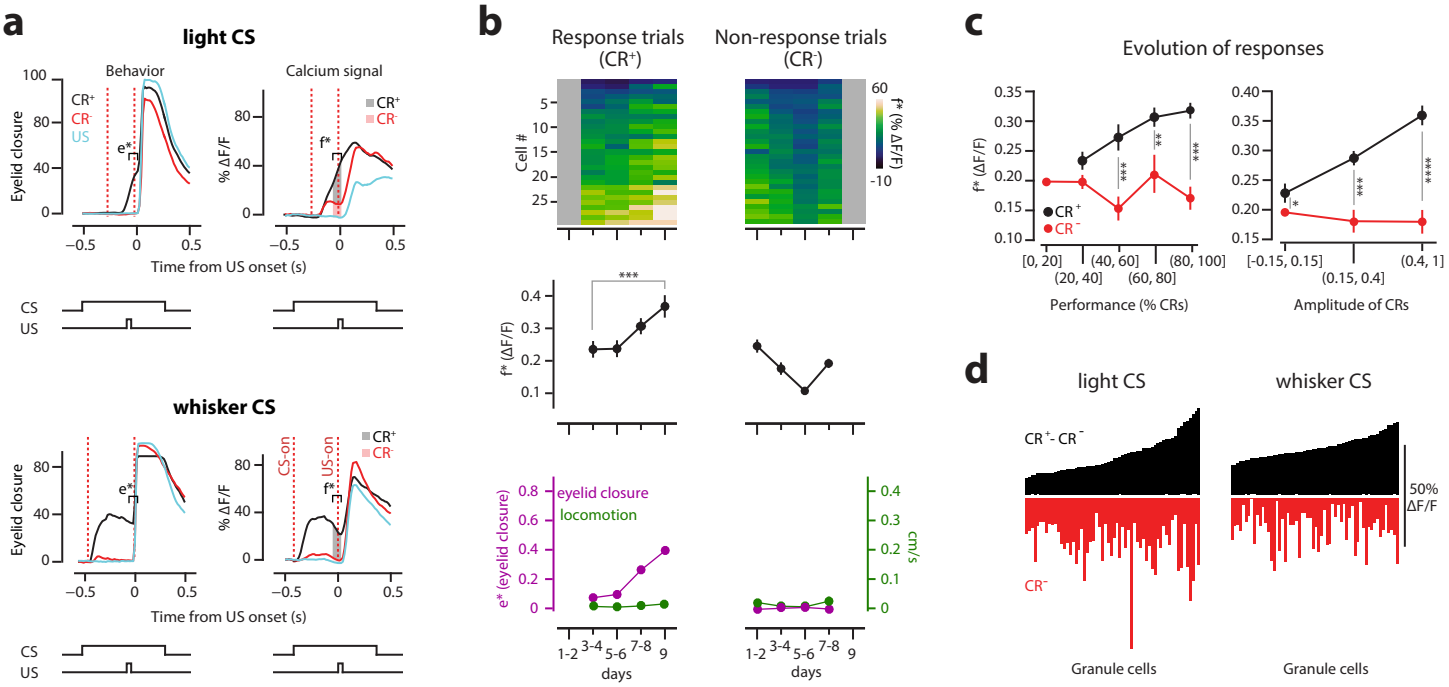

Figure 4: Cerebellar granule cells acquire a neural correlate of the learned conditional response. (**a**) *Top.* In a mouse trained with light CS, average CR amplitude (first column) and fluorescence responses (second column) for populations of granule cells grouped by trial type. US cyan, CR^+ trials black, and CR^- trials red. *Bottom*. Same results for a mouse trained with whisker CS. Behavioral and neural traces are averaged over a 85 msec time window preceding the UR for eyelid responses (e*) and fluorescence response (f*). Shaded regions in the right column represent the amount of GrC response in CR^- trials (red) and the excess GrC response in CR^+ vs. CR^- trials (black). (**b**) *Top.* Evolution of the calcium response during 9 days of conditioning to a CS light stimulus, shown separately for CR^+ (left) and CR^- (right) trials in 29 individual granule cells from a single animal. Gray indicates that not enough trials (5) were available to compute a value. *Middle*. Average calcium responses for the 29 granule cells in the population as a function of training day. *Bottom.* Eyelid response (purple) and locomotion (green) for CR^+ and CR^- trials. The error bars indicate ± SEM. (**c**) Evolution of GrC calcium responses across all animals. Plotted values show average and SEM calculated calculated by bootstrap-resampling to obtain equal weighting among field of views across six mice. *Left*, 0-20%, 20-40%, 40-60%, 60-80% and 80-100% of CRs. *Right*, blocks of trials sorted by e*. (**d**) Histograms of granule cell responses in 2 fully trained mice (one trained with whisker CS and one with light CS; for other mice see ED12d). Each histogram bar represents the response of a single granule cell to a CS stimulus without wheel movement. Red histograms show ΔF/F for trials with no conditional response (CR^-, same time bin as f*). Black histograms show difference in ΔF/F between CR^+ and CR^- trial responses for the same cells, i.e. the CR^+ excess (same time bin as f*). *, $p<0.05$. **, $p<0.01$. ***, $p<0.001$. ****, $p<0.0001$.

Figure 5

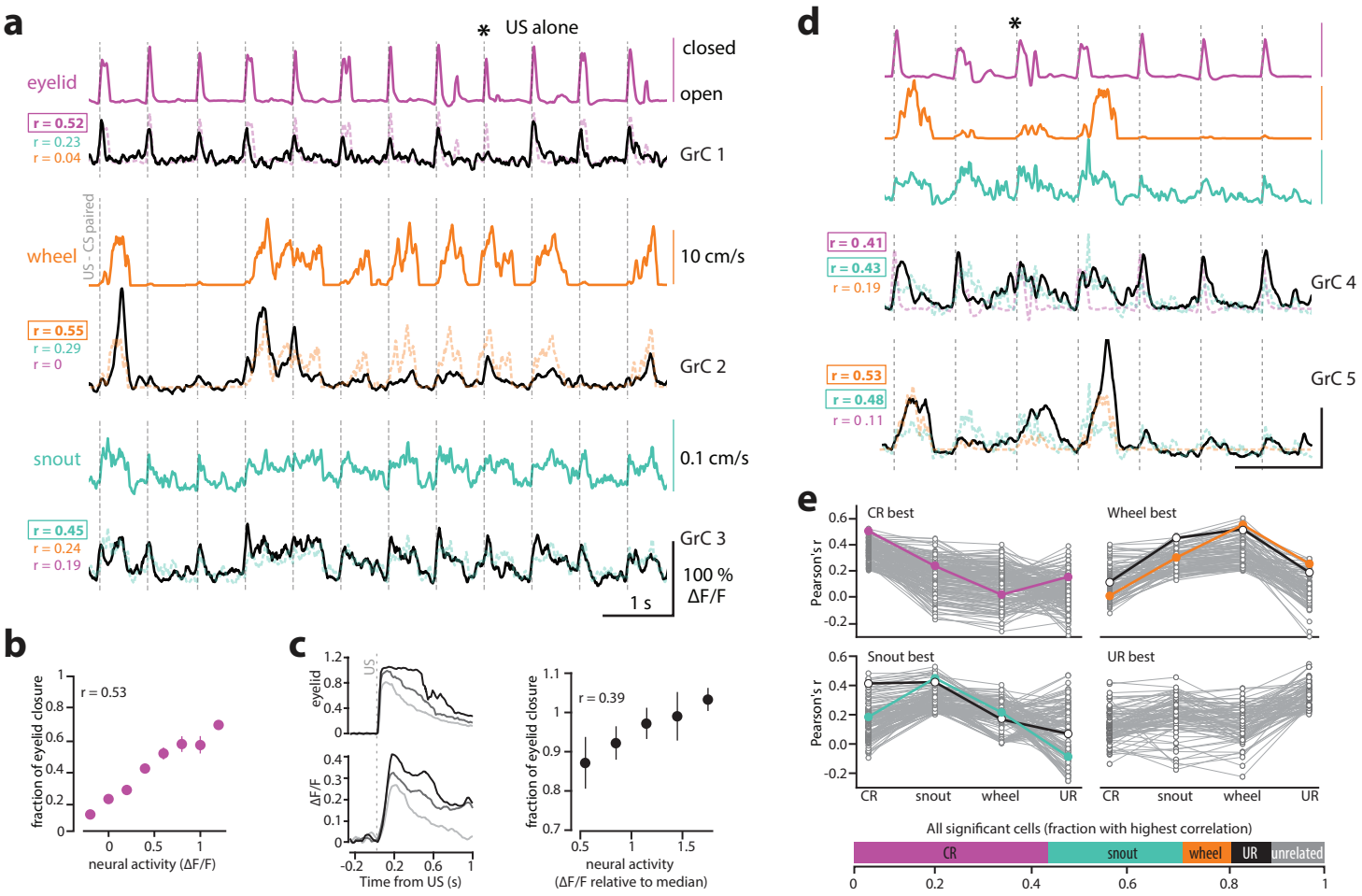

Figure 5: Granule cells simultaneously express correlates of eyeblink, locomotion, and snout movement.

(**a**) Simultaneous recording of three granule cells whose calcium signals (black) are correlated with eyelid (magenta), wheel (orange), or snout (cyan) movements. Pearson correlations over one day's recording session are given in the left column. Dashed traces superimposed on the calcium signals are the same movement-related traces shown in the panels above. (**b**) In a single granule cell, eyelid responses to conditional stimulus (CS) presentation (e*) as a function of fluorescence signal (f*). (**c**) *Left,* in a single granule cell, US-only presentation caused a range of eyelid response amplitudes (URs) concurrent with changes in f*. *Right,* eyelid closure amplitude as a function of neural activity, averaged across US-only trials. (**d**) Examples of granule cells with significant correlation to two behavioral parameters. (**e**) In three mice with the strongest learning and a high CR rate, tuning of all the imaged granule cells (gray lines) to conditional eyelid response (CR), snout movement, wheel speed, and unconditional eyelid response (UR) amplitude. The tuning corresponding to the GrCs in panels a (colored lines) and d (black lines) are highlighted. Bottom, the proportion of granule cells with strongest correlation to each individual behavior.

Figure 6

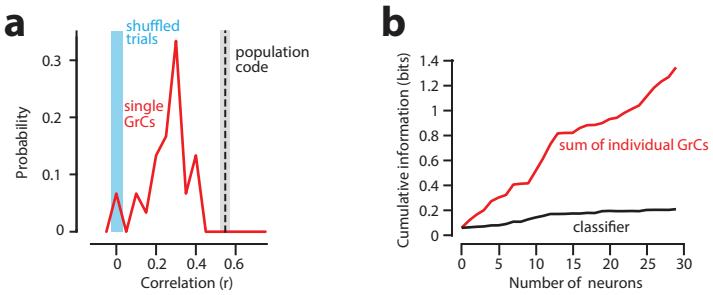

Figure 6: Redundancy in the granule cell representation of learned responses.
(**a**) For one example mouse, a histogram of Pearson correlations for all neurons (red, values larger than the shuffled range shown). The black dashed line indicates the Pearson correlation between the output of the population multivariate regressor and the actual eyelid response (e*) for multiple runs. Gray shading indicates the ±1 standard deviation range of regressor performance. The cyan band indicates the correlations for single cells when the eyelid responses in individual trials are randomly shuffled. (**b**) Information content of the population regressor (black) as a function of the number of neurons included. The red curve indicates the maximum possible information in the case of no redundancy.